JACS
JOURNAL OF THE AMERICAN CHEMICAL SOCIETY

ARTICLE

pubs.acs.org/JACS

Controlling the Self-Assembly Structure of Magnetic Nanoparticles and Amphiphilic Block-Copolymers: From Micelles to Vesicles

Robert J. Hickey,[†] Alyssa S. Haynes,[†] James M. Kikkawa,[‡] and So-Jung Park*[,†]

[†]Department of Chemistry, University of Pennsylvania, 231 South 34th Street, Philadelphia, Pennsylvania 19104, United States
[‡]Department of Physics, University of Pennsylvania, 209 South 33rd Street, Philadelphia, Pennsylvania 19104, United States

Supporting Information

ABSTRACT: We report how to control the self-assembly of magnetic nanoparticles and a prototypical amphiphilic block-copolymer composed of poly(acrylic acid) and polystyrene (PAA-*b*-PS). Three distinct structures were obtained by controlling the solvent−nanoparticle and polymer−nanoparticle interactions: (1) polymersomes densely packed with nanoparticles (magneto-polymersomes), (2) core−shell type polymer assemblies where nanoparticles are radially arranged at the interface between the polymer core and the shell (magneto-core shell), and (3) polymer micelles where nanoparticles are homogeneously incorporated (magneto-micelles). Importantly, we show that the incorporation of nanoparticles drastically affects the self-assembly structure of block-copolymers by modifying the relative volume ratio between the hydrophobic block and the hydrophilic block. As a consequence, the self-assembly of micelle-forming block-copolymers typically produces magneto-polymersomes instead of magneto-micelles. On the other hand, vesicle-forming polymers tend to form magneto-micelles due to the solubilization of nanoparticles in polymer assemblies. The nanoparticle−polymer interaction also controls the nanoparticle arrangement in the polymer matrix. In *N*,*N*-dimethylformamide (DMF) where PS is not well-solvated, nanoparticles segregate from PS and form unique radial assemblies. In tetrahydrofuran (THF), which is a good solvent for both nanoparticles and PS, nanoparticles are homogeneously distributed in the polymer matrix. Furthermore, we demonstrated that the morphology of nanoparticle-encapsulating polymer assemblies significantly affects their magnetic relaxation properties, emphasizing the importance of the self-assembly structure and nanoparticle arrangement as well as the size of the assemblies.

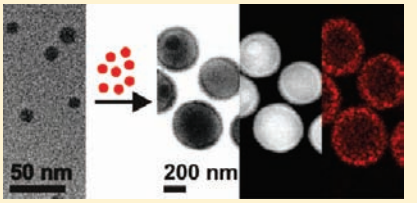

INTRODUCTION

Magnetic nanoparticles have been extensively studied for a range of biomedical applications including magnetic resonance imaging (MRI) and drug delivery.[1−7] Synthetic methods for monodispersed and stable magnetic nanoparticles have been well-established for organic phase oxide nanoparticles of various compositions, which typically utilize end-modified long chain aliphatic molecules such as oleic acids as surface binding agents.[8−10] Researchers have used various procedures to transfer the organic phase magnetic nanoparticles into water.[11−25] These techniques usually involve exchange of surface ligands,[2,6,20] silica coating,[11−14] or encapsulation of hydrophobic nanoparticles in amphiphilic molecules such as small surfactants,[24,26] lipids,[21,23] and block-copolymers.[13,15−19,22,25]

Amphiphilic polymers are particularly promising synthetic tools due to their stability, chemical diversity, controllable molecular weight, and useful mechanical properties.[27−32] Researchers have shown that self-assembly of amphiphilic block-copolymers and nanoparticles offers a powerful route to the formation of multifunctional nanoparticles for imaging and drug delivery applications.[1,26,33] For example, Taton and co-workers have demonstrated that hydrophobic iron oxide nanoparticles can be solubilized into micelles of block-copolymers composed of polystyrene (PS) and poly(acrylic acid) (PAA), where the amount of nanoparticles per micelle was controlled by varying the initial relative concentration of nanoparticles and polymers.[17] Gao and co-workers have encapsulated clusters of hydrophobic nanoparticles in the core of block-copolymer micelles.[15] Their transverse relaxivity rate (R_2) measurements revealed that polymer micelles packed with nanoparticles can be used as highly sensitive magnetic resonance probes. Berret and co-workers have prepared similar structures by mixing aqueous phase nanoparticles and block-copolymers.[16] They further demonstrated that R_2 of composite aggregates can be improved by increasing the size of nanoparticle clusters through the use of longer polymers.

Here, we report the formation of polymer vesicles (polymersomes),[29,30] densely packed with iron oxide nanoparticles in vesicle walls (Figure 1c). Furthermore, we reveal how to control the self-assembly structure of nanoparticle-encapsulating block-copolymer assemblies from micelles solubilizing magnetic nanoparticles (magneto-micelles, Figure 1b)[15,17,18] to (1) polymersomes packed with magnetic nanoparticles (magneto-polymersomes, Figure 1c) and (2) core−shell type assemblies where magnetic nanoparticles are radially localized at the interface between the polymer core and the shell (magneto-core shell, Figure 1a).[34−36] Polymersomes are technologically important and fundamentally interesting due to their ability to load both hydrophobic and hydrophilic substances by self-assembly.[28−30,37−39] A number of efforts have been made toward encapsulating several different types of nanoparticles into polymersome walls. For example, several

Received: October 6, 2010
Published: January 5, 2011

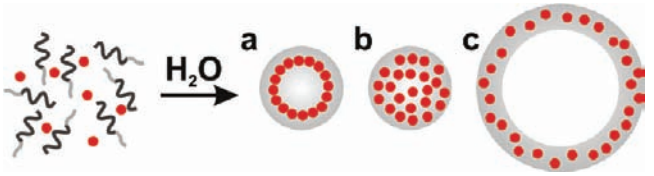

Figure 1. Self-assembly of nanoparticles and block copolymers. (a) Magneto-core shell assemblies formed when DMF/THF mixture (96.8% DMF) was used as the initial solvent for polymers and nanoparticles. (b) Magneto-micelles assembled in THF. (c) Magneto-polymersomes assembled in dioxane/THF (96.8% dioxane).

research groups (see work by Maskos and co-workers[40] and work by Binder and co-workers[41]) have incorporated quantum dots or gold nanoparticles in polymersomes by the film rehydration method. Forster and co-workers prepared oligolamella vesicles bridged by magnetic nanoparticles.[42] Eisenberg and co-workers recently reported an elegant approach to form well-defined polymersomes incorporated with metal nanoparticles coated with the same block-polymer as the vesicles.[43] However, in most previously reported well-defined polymersomes, the nanoparticle density in the vesicle wall was substantially lower than what has been achieved for micelles. In the studies where the nanoparticle loading density was high, the assemblies were nonuniform and the vesicle structure was difficult to discern.[19,41] It is also worth noting that Eisenberg's recent report[43] stated that their attempts to incorporate PS-modified nanoparticles into the PS wall of PAA-*b*-PS polymersomes did not succeed. Due to the difficulties, most previous work on the self-assembly of amphiphilic block-copolymers and magnetic nanoparticles was performed with micelles[17,18] or irregular polymer/nanoparticle aggregates[16,25] as mentioned above. To the best of our knowledge, this report is the first to describe well-defined polymersomes densely packed with iron oxide nanoparticles. We have previously reported the radial nanoparticle assembly structure (referred to as magneto-core shell) depicted in Figure 1a.[34−36] The magneto-micelles shown in Figure 1b were prepared by following the procedure reported by Taton and co-workers.[17,18,44] Although the two structures shown in Figure 1a, b were previously reported, it has not been understood what leads to the two distinct structures.

Here, we show that while well-established self-assembly principles of amphiphilic block-copolymers[27,28,31,38,45−50] provide a valuable guideline for the preparation of nanoparticle-encapsulating block-copolymer assemblies, they do not directly apply to the simultaneous self-assembly of nanoparticles and block-copolymers. This aspect is especially important when it is desirable to achieve high density nanoparticle loading in polymer assemblies. The study described here reveals how the incorporation of nanoparticles affects the self-assembly structure and how to control the morphology of nanoparticle-encapsulating polymer assemblies. Furthermore, we demonstrate for the first time that the morphology of nanoparticle-encapsulating polymer assemblies significantly affects their magnetic relaxation properties, underscoring the importance of the self-assembly structure and nanoparticle arrangement as well as the size of the assemblies.

RESULTS AND DISCUSSION

Solvent Effect on the Self-Assembly Structure. The oleic acid-stabilized iron oxide nanoparticles (diameter: 5.6 ± 0.5 nm) were prepared by a modified literature procedure.[10] The synthesized magnetic nanoparticles were self-assembled with a prototypical

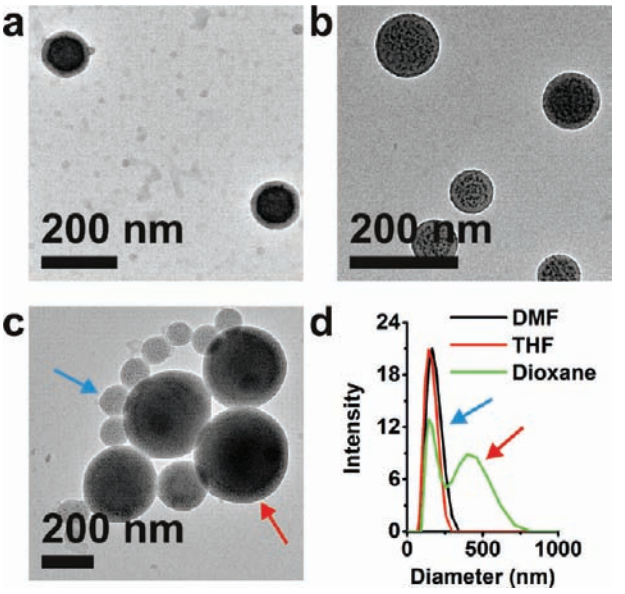

Figure 2. Various morphologies of nanoparticle-encapsulating block-copolymer assemblies formed in three different solvent systems with 5.6 nm particles and PAA_{38}-*b*-PS_{154} at the nanoparticle mass percent of 15.9%. Same types of morphologies were observed for PAA_{38}-*b*-PS_{154} and PAA_{38}-*b*-PS_{189}. (a) A TEM image of magneto-core shell assemblies formed when DMF/THF (96.8 vol % DMF) was used as the initial solvent for polymers and nanoparticles. (b) A TEM image of magneto-micelles assembled with THF as the initial solvent. (c) A TEM image of coassemblies formed with dioxane/THF (96.8 vol % dioxane) as the initial solvent, showing that both magneto-micelles (blue arrow) and magneto-polymersomes (red arrow) were formed. (d) DLS data for the assemblies formed with three different solvents. The diameters of the assemblies were measured to be 164 ± 14 and 142 ± 11 nm for DMF and THF samples, respectively. The dioxane sample was composed of two species, magneto-micelles (blue arrow) and magneto-polymersomes (red arrow). The size of magneto-micelles and magneto-polymersomes were measured to be 166 ± 18 and 408 ± 46 nm.

amphiphilic block-copolymer of PAA-*b*-PS without further surface modifications. For all experiments, self-assembly was carried out by the cosolvent method (Figure 1). Briefly, block-copolymers and nanoparticles were first mixed in a cosolvent. Then, 600 μL of water was slowly added to the solution at the rate of 10 μL/30 s for 30 min to induce the self-assembly of block-copolymers and nanoparticles. The resulting coassemblies were dispersed in water by dialysis and centrifugation. The structure of the prepared coassemblies was characterized by transmission electron microscopy (TEM), scanning transmission electron microscopy (STEM), energy-dispersive X-ray spectroscopy (EDS), electron energy loss spectroscopy (EELS), and dynamic light scattering (DLS).

To examine the solvent effect on the self-assembly structure, we used three different solvents [*N*,*N*-dimethylformamide (DMF), tetrahydrofuran (THF), or 1,4-dioxane (dioxane)] to dissolve polymers (PAA_{38}-*b*-PS_{154}) (Figure 2). The polymers dissolved in three different solvents (1500 μL) were mixed with nanoparticles (5.6 nm iron oxide particles) dispersed in a small amount of THF (50 μL). For all three samples, the nanoparticle mass percent was kept constant at 15.9%. Figure 2 presents TEM images of three distinct morphologies obtained with the different solvent systems. The compositions of the cosolvents before the water addition were DMF/THF mixture (96.8 vol % DMF), THF (100% THF), and dioxane/THF mixture (96.8 vol % dioxane)

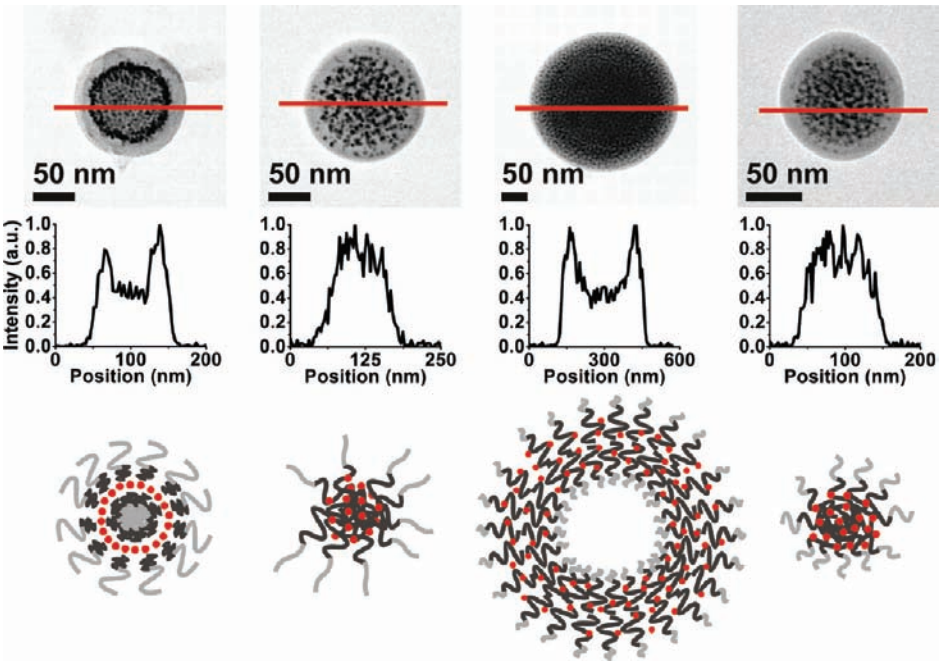

Figure 3. Structural characterization of three different self-assembly structures. STEM images and Fe intensity line scans for (a) magneto-core shell assemblies formed in DMF/THF (96.8% DMF), (b) magneto-micelles formed in THF, (c) magneto-polymersomes formed in dioxane/THF (96.8% dioxane), and (d) magneto-micelles formed in dioxane/THF (96.8% dioxane). The assemblies were prepared with PAA_{38}-*b*-PS_{189} at the polymer concentration of 0.04 wt % and a nanoparticle mass percent of 27.1%. The self-assembled structures are pictorially described below the EDS data, where light gray lines, dark gray lines, and red dots represent PAA, PS, and nanoparticles, respectively.

for the assemblies presented in Figure 2a,b,c, respectively. As we have previously reported, radial nanoparticle assemblies (magneto-core shell) were formed in DMF/THF (96.8 vol% DMF) (Figures 1a, 2a).[34−36] The magneto-core shell structure is composed of a polymer core, a polymer shell, and a monolayer of magnetic nanoparticles entrapped at the interface between the polymer core and the shell. The polymer core is composed of one or multiple reverse micelles, and the nanoparticle-decorated polymer core is stabilized in water by the polymer shell, which consists of a layer of block-copolymers. The polymer morphology in magneto-core shell assemblies resembles that of large compound micelles reported by Eisenberg and co-workers,[49] except that the core−shell structure encapsulating nanoparticles possesses fairly narrow polydispersity (8.5% by DLS) while large compound micelles typically have very broad size distributions.[49] When THF was used as an initial solvent, nanoparticle-loaded polymer micelles (magneto-micelles) were obtained as reported by Taton and co-workers (Figure 2b).[17] In this structure, iron oxide nanoparticles were homogeneously distributed in the polymer matrix. The DLS data presented in Figure 2d showed that the magneto-micelles (Figure 2b) and magneto-core shell assemblies (Figure 2a) possess similar size and size distributions. When dioxane/THF (96.8% dioxane) was used as an initial solvent, a mixture of magneto-micelles and magneto-polymersomes was obtained (Figure 2c). Consistent with the TEM result, the DLS data for the dioxane sample exhibited a dual distribution; the two peaks at 166 ± 18 and 408 ± 46 nm were assigned for magneto-micelles (blue arrow) and magneto-polymersomes (red arrow), respectively.

The arrangement of nanoparticles in the three different structures was further examined by EDS (Figure 3). The Fe intensity line scan of magneto-core shell structure showed higher iron intensities at the spherical interface between the polymer core and the shell, confirming the radial arrangement of nanoparticles (Figure 3a). Note that nanoparticles appear to be in the core part in the TEM image (Figure 3a) only because TEM images are two-dimensional projections of three-dimensional objects. The dark contrast at the spherical interface is indicative of selective accumulation of nanoparticles at the spherical interface.[36] On the contrary, the Fe line scan of the THF sample (magneto-micelles) exhibited a Gaussian curve, which indicates that nanoparticles are homogeneously distributed in the polymer matrix (Figure 3b). The magneto-micelles found in the dioxane sample showed the similar Fe intensity profile (Figure 3d). As expected, magneto-polymersomes in the same dioxane sample exhibited high Fe intensities in the polymersome wall due to the hollow structure (Figure 3c). The overall Fe intensity profile of magneto-polymersomes was similar to that of magneto-core shell assemblies. However, the Fe intensity peak of magneto-core shell assemblies was sharper than that of magneto-polymersomes with full width at half-maximum of 17.0 ± 4.8 and 59.8 ± 9.3 nm for core−shell and polymersomes, respectively (see Supporting Information, Figure S2). This result is consistent with the TEM observations that nanoparticles form a monolayer in magneto-core shell assemblies while in magneto-polymersomes nanoparticles are distributed throughout the polymer wall. The structures of the three distinct assemblies are pictorially described below the EDS data in Figure 3.

The self-assembled structures of PAA-*b*-PS (PAA_{38}-*b*-PS_{154}, PAA_{38}-*b*-PS_{189}) formed without nanoparticles were micelles, micelles, and vesicles for DMF/THF (96.8% DMF), THF, and dioxane/THF (96.8% dioxane), respectively, which are consistent with the previously reported results.[48] It is well-known that the solvent−polymer interaction is an important factor that determines the self-assembly structure of amphiphilic block-copolymers.[48] Extensive studies by Eisenberg and co-workers[48] showed that the

dx.doi.org/10.1021/ja1090113 |*J. Am. Chem. Soc.* 2011, 133, 1517–1525

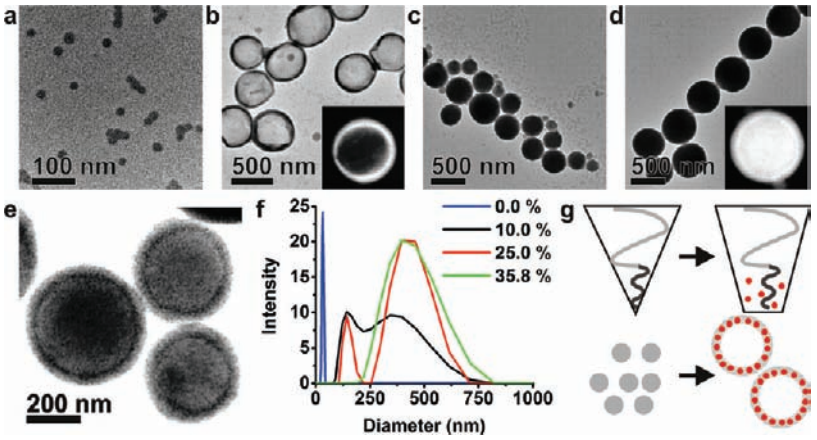

Figure 4. Effect of nanoparticles on the self-assembly structure of block-copolymers (PAA_{38}-*b*-PS_{73}) and nanoparticles (5.6 nm nanoparticle). (a) A TEM image of block-copolymers formed without nanoparticles showing simple micelles. (b−d) TEM images of coassemblies formed at different nanoparticle mass percents [(b) 10.0%, (c) 25.0%, (d) 35.8%]. The assemblies were formed in dioxane/THF (96.8% dioxane) at a constant polymer concentration (0.03 wt %) with varying the nanoparticle mass percent. Insets in parts b and d are dark-field STEM images. (e) A bright field STEM image of maneto-polymersomes shown in part d. Vesicle structures are clearly seen in the bright field STEM image. (f) DLS data of the four different samples presented in a−d. Consistent with the TEM results, the DLS data show that the assemblies formed at 10.0% and 25.0% nanoparticle mass percents are composed of magneto-polymersomes and magneto-micelles, and the assemblies formed at 35.8% nanoparticle mass fraction contains only magneto-polymersomes. (g) A pictorial description of the relative volume ratio change caused by the addition of nanoparticles (top), inducing the micelle-to-vesicle morphological change (bottom).

degree of stretching for PS is the greatest in THF and the smallest in DMF (THF > dioxane > DMF) as predicted from the solubility parameters (δ) (see Supporting Information, Table S1) and observed in the experimental data.[48] Both the solubility parameters and the dielectric constant of solvents should be considered for a charged polymer, PAA. The dielectric constants listed in Table S1 predict that the average surface area per corona chain (A_c) is the greatest in DMF and the smallest in dioxane due to the charge repulsion between PAA strands in a high dielectric medium. Thus, the degree of PAA chain stretching is the largest in dioxane.[48] Consequently, the relative volume taken up by PAA becomes the largest in DMF and the smallest in dioxane (DMF > THF > dioxane), which explains the formation of micelles in DMF and THF and vesicles in dioxane without nanoparticles.[48] Thus, when nanoparticles are passively incorporated, they are expected to form magneto-micelles in THF and magneto-polymersomes in dioxane. The TEM and DLS data presented in Figure 2 show that the expected structures were indeed formed in THF and dioxane/THF (96.8% dioxane). However, it is important to note that magneto-polymersomes were not the major product of the dioxane sample. The polymersome peak of the DLS data presented in Figure 2 appears to be substantial only because bigger polymersomes scatter light more strongly than smaller micelles. When the DLS data shown in Figure 2 was converted into the number distribution, the vesicle population was rather small (Supporting Information, Figure S3). Also note that unique radial assemblies were formed instead of typical micelles when DMF/THF (96.8% DMF) was used as the initial solvent. These results underscore that it is important to consider the effect of nanoparticles on the self-assembly formation in order to obtain the hybrid particle with the desired structure and properties (see below).

Magneto-Polymersomes: The Incorporation of Nanoparticles Changes the Morphology of Coassemblies. Uniform polymersomes packed with magnetic nanoparticles were prepared with PAA_{38}-*b*-PS_{73} using dioxane/THF (96.8% dioxane) as the initial solvent (Figure 4d). When PAA_{38}-*b*-PS_{73} is self-assembled under the same condition without nanoparticles, it forms simple micelles as shown in the TEM image and the DLS data (Figure 4a, f). However, even at low nanoparticle mass percents (10.0%), magneto-polymersomes emerge along with magneto-micelles (Figure 4b,f). The magneto-polymersome population was increased with the mass percent of nanoparticles (Figure 4b−d,f). Finally magneto-polymersomes became the only species of the sample at the nanoparticle mass percent of 35.8% (Figure 4d,f). The vesicle structure is well visualized in the bright-field STEM image presented in Figure 4e. We attribute the nanoparticle-induced micelle-to-vesicle morphological change to the relative volume change between the hydrophobic and hydrophilic part of block-copolymers. The incorporation of nanoparticles increases the effective volume taken up by PS, and the relative volume ratio between the hydrophilic (PAA) and the hydrophobic (PS and nanoparticles) parts becomes more symmetric and appropriate for vesicle formation as depicted in Figure 4g. Similar phenomena have been observed in thin film studies.[51]

The incorporation of nanoparticles also affects the mechanical properties of polymersomes. Most magneto-polymersomes formed at low nanoparticle mass percents were collapsed on the TEM grid as evidenced by the distinctively dark contrast at the edges (Figure 4b). However, the majority of magneto-polymersomes formed at 35.8% nanoparticle mass percent maintained the spherical shape when dried on a TEM grid (Figure 4d), indicating that nanoparticles rigidify the vesicles. The structures of polymersomes formed at two different nanoparticle mass percents (10.0%, 35.8%) were further characterized using EELS and EDS (Figure 5). High magnification STEM images show that polymersomes are packed with magnetic nanoparticles and that the nanoparticle density increases with the nanoparticle mass percent (Figure 5a,b). The relative height profile measured by the electron scattering intensity obtained from EELS confirms that the magneto-polymersomes formed at 35.8% nanoparticle mass percent indeed maintained their shape while the magneto-polymersomes formed at 10.0% nanoparticle mass percent were collapsed on the TEM

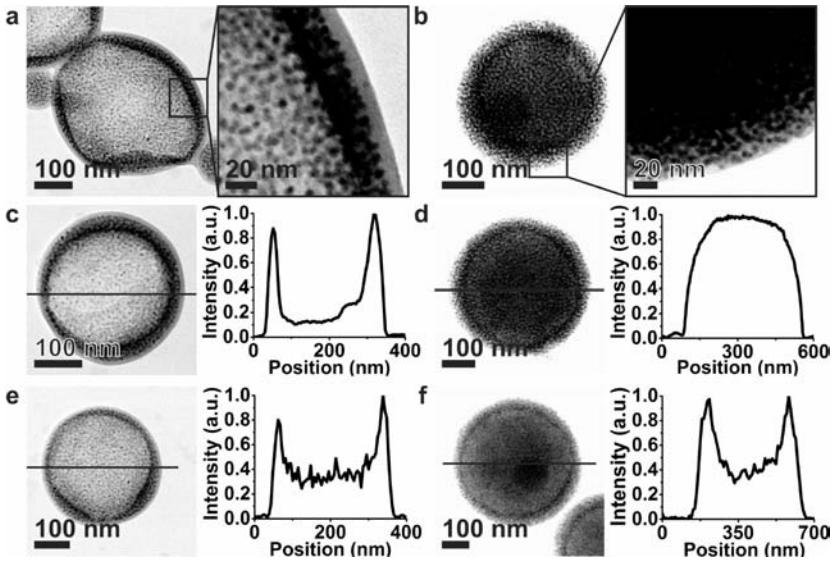

Figure 5. Structural characterization of magneto-polymersomes presented in Figure 4b,d, which were formed at two different nanoparticle mass percents [(a,c,e) 10.0%, (b,d,f) 35.8%)] (a,b) Bright-field STEM images of magneto-polymersomes formed at a (a) nanoparticle mass percent of 10.0% and a (b) nanoparticle mass percent of 35.8%. (c,d) EELS relative height profiles for assemblies formed at a (c) nanoparticle mass percent of 10.0% and at a (d) nanoparticle mass percent of 35.8%. (e,f) EDS Fe intensity profiles for assemblies formed at a (e) nanoparticle mass percent of 10.0% and at a (f) nanoparticle mass percent of 35.8%.

grid (Figure 5c,d). The collapsed structure is evidenced by the bowl shape height profile of polymersomes (Figure 5c). Finally, the EDS analysis for iron showed similar line intensity profiles regardless of the nanoparticle density because nanoparticles are located in the wall of polymersomes in both cases (Figure 5e,f). It is also interesting to note that when the nanoparticle mass percent is low, nanoparticles were preferentially located in the center of polymersome walls and the outer part (~8 nm) of the vesicle wall is clear of nanoparticles (Figure 5a). Eisenberg and co-workers recently reported the formation of polymersomes where metal nanoparticles were located in the center portion of polymersomes.[43] In the approach, nanoparticles surrounded by the same block-copolymers as the polymersomes were used for the incorporation of nanoparticles in the center of polymersome walls. Note that, in our study, no nanoparticle functionalization was needed to localize nanoparticles in the center part of the vesicle wall.

As mentioned above, the yield of magneto-polymersomes was low when nanoparticles were self-assembled with vesicle-forming polymers (e.g., PAA_{38}-*b*-PS_{154} and PAA_{38}-*b*-PS_{189}) (Figure 1c,d). In fact, the number ratio between magneto-polymersomes and magneto-micelles increases with increasing PAA/PS mole ratio when the assemblies were formed at the same polymer concentration (0.03 wt %) and nanoparticle mass percent (35.8%) (Figure 6). This trend is opposite of what is expected for the self-assembly of block-copolymers in the absence of nanoparticles;[52] again, without nanoparticles, micelles were formed with a short polymer of PAA_{38}-*b*-PS_{73}, and vesicles were formed with longer polymers of PAA_{38}-*b*-PS_{154} and PAA_{38}-*b*-PS_{189}.

To understand this behavior, vesicle-forming polymers (PAA_{38}-*b*-PS_{154}) were self-assembled with nanoparticles at a series of different nanoparticle mass percents (Figure 7). The self-assembly conditions were kept the same for the two sets of experiments presented in Figures 4 and 7 except the length of PS. Interestingly, at low nanoparticle mass percents (5.3%, 10.0%), vesicle-forming polymers of PAA_{38}-*b*-PS_{154} (Figure 7a) generated magneto-micelles

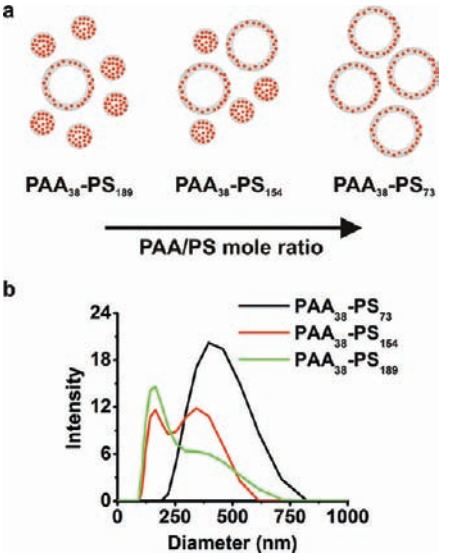

Figure 6. (a) Pictorial description of the polymer length dependence on the self-assembly structure. With decreasing PS lengths, magneto-polymersomes become dominant over magneto-micelles. (b) DLS data of coassemblies formed with three different length polymers (PAA_{38}-*b*-PS_{73}, PAA_{38}-*b*-PS_{154}, and PAA_{38}-*b*-PS_{189}). All self-assembly conditions were kept constant with a nanoparticle mass percent of 35.8% and the polymer concentration of 0.03 wt %. The DLS data indicate that the population of magneto-polymersomes increases with decreasing PS length as depicted in part a.

(Figure 7b,f). Magneto-polymersomes were not found in the samples as evidenced by the single DLS peak corresponding to magneto-micelles (Figure 7f). This behavior can be explained by the solubilization of nanoparticles in the polymer assemblies, which reduces the polymer stretching of the outer polymer layer. As nanoparticles are incorporated into the core, PS of the outer polymer layer does not have to stretch to form micelles of the size

dx.doi.org/10.1021/ja1090113 |*J. Am. Chem. Soc.* 2011, 133, 1517–1525

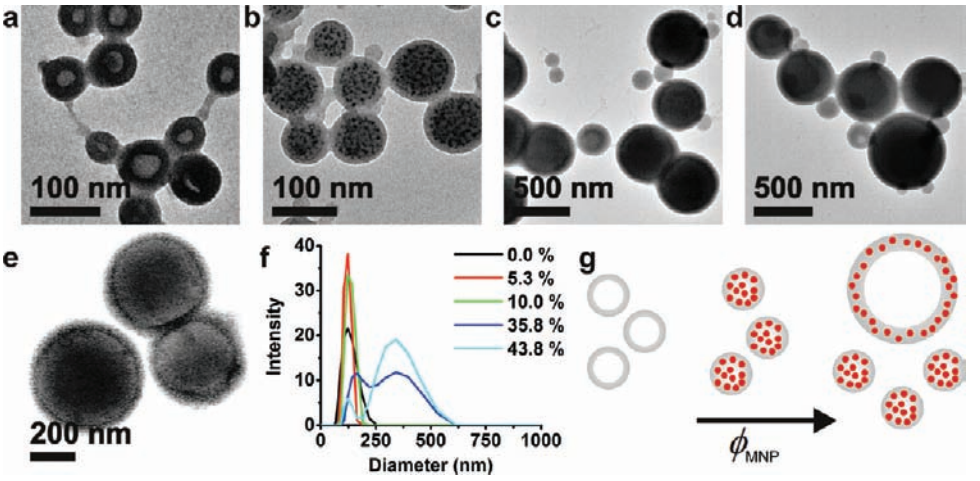

Figure 7. Effect of nanoparticle mass percents on the self-assembly structure of a vesicle-forming polymer, PAA_{38}-*b*-PS_{154} (0.03 wt %) and 5.6 nm particles. (a) A TEM image of block-copolymers formed without nanoparticles showing vesicles. (b−d) TEM images of coassemblies formed at different nanoparticle mass percents [(b) 10.0%, (c) 35.8%, (d) 43.8%]. The assemblies were formed in dioxane (96.8%) at a constant polymer concentration (0.03 wt %) with varying the nanoparticle mass percent. (e) A bright field STEM image of magneto-polymersomes shown in part c. Vesicle structures are clearly seen in the image. (f) DLS data of the four different samples presented in parts a−d. Consistent with the TEM images, the DLS data show that, at low nanoparticle mass percents, magneto-micelles were formed. At higher nanoparticle mass percents, a mixture of magneto-polymersomes and magneto-micelles were formed. (g) A pictorial description of the effect of nanoparticle mass precent on the self-assembly structure of vesicle-forming polymers.

of vesicles. Thus, the introduction of nanoparticles induces the morphological change from hollow vesicles to filled micelles. The same behavior has been observed for the self-assembly of vesicle-forming PAA-*b*-PS in the presence of PS homopolymers.[49] The observation that the diameter of the assemblies do not significantly change from polymersomes (Figure 7f, black) to magneto-micelles (Figure 7f, red, green) is consistent with the explanation. At higher nanoparticle mass percents, magneto-polymersomes are also formed along with magneto-micelles (Figure 7c,d). As shown in the DLS data (Figure 7f), the number ratio of magneto-polymersomes over magneto-micelles increased with the nanoparticle mass percents. This behavior can be explained by the same rationalization used to explain the formation of magneto-polymersomes from micelle-forming polymers (Figure 4); at high nanoparticle mass percents, incorporated nanoparticles increase the relative volume of the hydrophobic block, favoring the formation of magneto-polymersomes with a smaller radius of curvature than magneto-micelles and polymersomes formed without nanoparticles. Figure 7g summarizes the morphology change of vesicle-forming polymers with the incorporation of nanoparticles. At low nanoparticle mass percents, nanoparticles act as solutes, and they are solubilized into the core of vesicles, forming magneto-micelles. At high nanoparticle mass percents, magneto-polymersomes emerge along with magneto-micelles with an increasing number of polymersomes with the amount of nanoparticles. Because longer polymers can solubilize larger amounts of nanoparticles,[53] vesicle-forming polymers with long PS chains require larger amounts of nanoparticles to form magneto-polymersomes (Figure 7). On the contrary, micelle-forming polymers with short PS chains generate magneto-polymersomes even at low nanoparticle mass percents because the short polymers cannot solubilize a large amount of nanoparticles without morphological change (Figure 4). Thus, when the nanoparticle mass percent was kept constant, block-copolymers with short PS chain provide higher yields of magneto-polymersomes (Figure 6). Moreover, magneto-polymersomes formed with micelle-forming polymers (Figure 4) were more uniform than those formed with longer, vesicle-forming polymers.

Magneto-Core Shell Assemblies and Magneto-Micelles: Solvent Effect on Nanoparticle Distribution and Hybridization. The unique radial arrangement of nanoparticles in magneto-core shell assemblies (Figure 1a) can be explained by the solvent effect. As mentioned above, PS has a compact structure in DMF while it is well-solvated in THF. Thus, nanoparticles cannot be solubilized well in the PS matrix when the assemblies were formed in DMF/THF (96.8% DMF). Thus, nanoparticles are pushed out of PS and accumulated at the spherical interface between the polymer core and the shell, forming a monolayer at the spherical interface as depicted in Figure 3a. On the contrary, in THF and dioxane, nanoparticles can be incorporated as solutes into the swollen PS matrix as expected from their solubility parameters (Table S1). Thus, nanoparticles are distributed throughout the polymer micelles or vesicle walls (Figure 3b,c).

Nanoparticle−solvent interactions are also important, and they affect the nanoparticle hybridization in the polymer matrix. Figure 8 presents the self-assembly structures formed with two different sized iron oxide nanoparticles (diameters determined by TEM: 5.6 ± 0.5 nm and 14.9 ± 0.9 nm) in DMF/THF (96.8% DMF) or THF. For one experiment shown in Figure 8a, two different sized nanoparticles were separately mixed with polymers in DMF/THF (96.8% DMF). The two solutions were then mixed together for self-assembly. Interestingly, the two different sized nanoparticles were kept separated in the final self-assembled structures in water and no single assembly was found to have both nanoparticles (Figure 8a). This segregation phenomenon can be explained by the solvent−nanoparticle interaction. Due to the poor solubility of nanoparticles in DMF, nanoparticles are associated with polymers even before the addition of water[35] and two different sized nanoparticles stay segregated in different polymer assemblies. When desired, magneto-core shell assemblies with mixed nanoparticles can be prepared by combining two different sized nanoparticles before mixing them with

dx.doi.org/10.1021/ja1090113 |*J. Am. Chem. Soc.* 2011, 133, 1517–1525

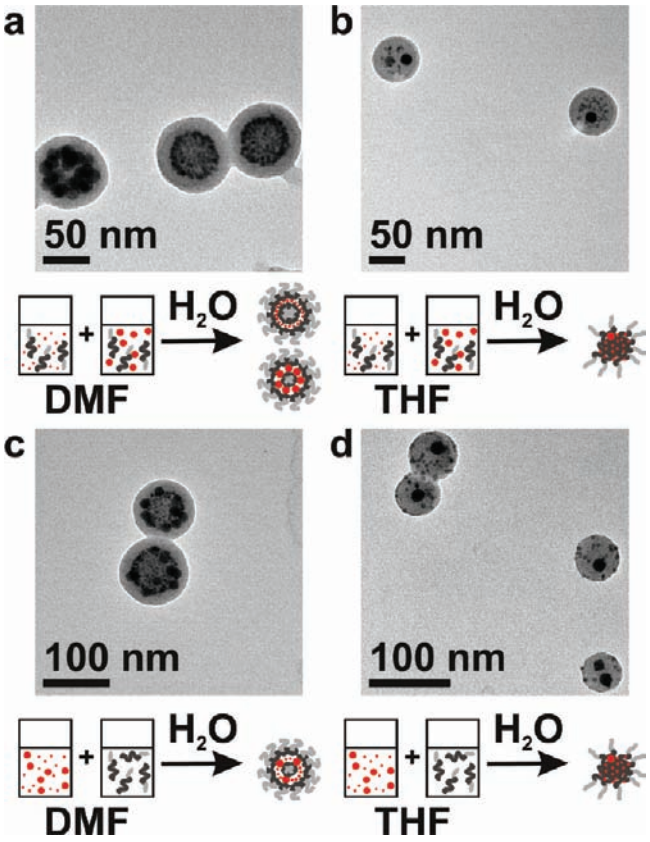

Figure 8. Solvent effect on the nanoparticle arrangement and hybridization. Two different sized iron oxide nanoparticles (5.6 and 14.9 nm in diameter) were self-assembled with PAA_{38}-*b*-PS_{247} (0.01 wt %) at a nanoparticle mass percent of 24.4% using DMF/THF (96.8% DMF) or THF as initial solvents. (a,c) Magneto-core shell assemblies formed in DMF/THF (96.8% DMF). When two different sized nanoparticles were mixed with polymers before combining the two particles together, different sized particles were (a) segregated in different assemblies, while when two different sized nanoparticles were combined before mixing with polymers, (b) assemblies with mixed nanoparticles were formed. (b,d) Magneto-micelles formed in THF. Regardless of the order of mixing, magneto-micelles with both nanoparticles were formed.

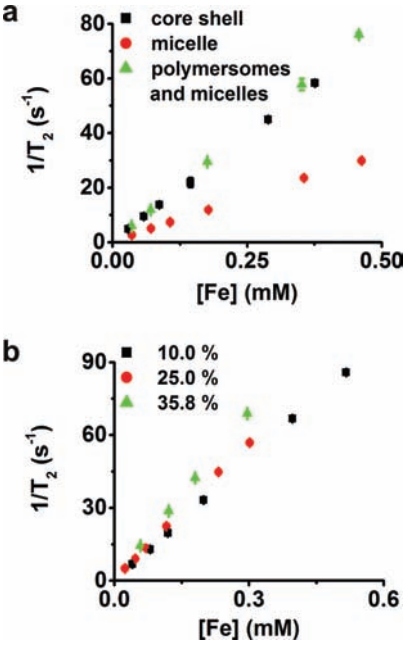

Figure 9. Inverse transverse relaxation time ($1/T_2$) versus the iron molar concentration [Fe] for nanoparticle-encapsulating block-copolymer assemblies. (a) Magnetic relaxivity data for three different assemblies shown in Figure 2a−c, which were prepared by self-assembling 5.6 nm particles and PAA_{38}-*b*-PS_{154} at a constant nanoparticle mass percent of 15.9% in three different solvents. Magneto-core shell assemblies (black) and magneto-micelles (red) were formed using DMF/THF (96.8% DMF) and THF, respectively. The assemblies formed in dioxane consist of magneto-polymersomes and magneto-micelles (green). (b) Magnetic relaxivity data for magneto-polymersomes presented in Figure 4b−d, which were prepared by self-assembling PAA_{38}-*b*-PS_{73} and nanoparticles at different nanoparticle mass percents, 10.0% (black), 25.0% (red), and 35.8% (green). The error bars are the standard deviations from three different measurements.

polymers (Figure 8c). Thus, when DMF/THF (96.8% DMF) was used as the initial solvent, the order of mixing influences the nanoparticle hybridization. In contrast, when THF was used as the initial solvent, micelles with both nanoparticles were formed regardless of the order of mixing, because THF is a good solvent for both nanoparticles and PS (Figure 8b,d).

Transverse Relaxivity Measurements for Magnetic Resonance Imaging (MRI). To evaluate the potential use of magneto-polymersomes in MRI imaging, R_2 values were measured for the three different types of assemblies encapsulating nanoparticles. Transverse (T_2) relaxivity times of the protons of water in the aqueous solutions of magneto-polymersomes were determined using a Bruker mq60 MR relaxometer operating at 1.41 T (60 MHz). The measured inverse relaxation times ($1/T_2$) were plotted as a function of iron concentration [Fe] (Figure 9).

First, R_2 values were measured for the three different types of assembly structures presented in Figure 2 in order to examine the impact of nanoparticle arrangement and the overall morphology on the magnetic relaxivity (Figure 9a). The R_2 values determined from the slopes of the plots[16] in Figure 9a were 154 ± 1, 64 ± 1, and 167 ± 1 s^{-1} mM^{-1} for DMF/THF (96.8% DMF) (magneto-core shell assemblies), THF (magneto-micelles), and dioxane/THF (96.8% dioxane) (mixture of magneto-micelles and magneto-polymersomes) samples, respectively. This result indicates that the R_2 significantly varies depending on the self-assembly structure. Note that the magneto-core shell structure showed a significantly higher relaxivity rate than the simple micelles, although the sizes of the two assemblies were similar, and they were prepared at the same nanoparticle mass percent of 15.9% (Figure 2d). In magneto-core shell assemblies, all nanoparticles are packed at the interface between the polymer core and the shell, and located close to the surrounding water. Since MRI is based on the magnetic relaxivity rates of surrounding water molecules, the water accessibility of contrast agents is an important factor that affects the relaxivity rates and resulting MRI contrasts.[4] In magneto-micelles assembled in THF, nanoparticles are homogeneously distributed, and the nanoparticle population is high in the core, which is farther away from water (Figure 3b). This explains the greater relaxivity rate observed for the magneto-core shell structure. Magneto-polymersomes contain a larger number of nanoparticles per assembly than the magneto-core shell structure, and they have excellent water accessibility owing to the hollow structure. Indeed, the dioxane sample, which contained magneto-micelles and magneto-polymersomes, showed R_2 values comparable to that of magneto-core shell assemblies, implying

dx.doi.org/10.1021/ja1090113 |*J. Am. Chem. Soc.* 2011, 133, 1517–1525

that magneto-polymersomes have a higher relaxivity rate than magneto-core shell structures. Note that our study described here demonstrated for the first time that the overall morphology of hybrid nanostructures and the nanoparticle arrangement in the polymer matrix significantly influence the R_2 relaxivity rates as well as the size of the assemblies and the degree of nanoparticle aggregation.[2,16,22,23]

Relaxivity rates were also measured for the magneto-polymersomes presented in Figure 4. The R_2 values were calculated to be 167 ± 1, 187 ± 1, and 228 ± 4 s^{-1} mM^{-1} for assemblies made at nanoparticle mass percents of 10.0%, 25.0%, and 35.8%, respectively (Figure 9b). The magneto-polymersomes formed at 35.8% nanoparticle mass percent have a higher R_2 value than previously reported values[4] for similar sized iron oxide nanoparticles including a clinically approved commercial product [Ferucarbotran (Resovist): 186 mM^{-1} s^{-1}].[4]

CONCLUSIONS

We investigated how nanoparticles affect the self-assembly structure of a prototypical amphiphilic polymer of PAA-*b*-PS and as-synthesized, oleic acid stabilized magnetite nanoparticles. Three distinct assembly structures were obtained by controlling the solvent−nanoparticle and polymer−nanoparticle interactions: (1) polymersomes where nanoparticles are packed in the wall (magneto-polymersomes), (2) core−shell type polymer assemblies where nanoparticles are radially arranged at the interface between the polymer core and the shell (magneto-core shell), and (3) polymer micelles where nanoparticles are homogeneously incorporated (magneto-micelles).

The type of solvent and nanoparticle−polymer interaction greatly affect the overall morphology and the nanoparticle arrangement in the polymer matrix. Three different solvents [i.e., DMF/THF (96.8% DMF), THF, dioxane/THF (96.8% dioxane)] were used to self-assemble PAA_{38}-*b*-PS_{154} and magnetic nanoparticles. The assembly structures prepared in the absence of nanoparticles were micelles, micelles, and vesicles for DMF/THF (96.8% DMF), THF, and dioxane/THF (96.8% dioxane), respectively. In THF, which is a good solvent for both PS and nanoparticles, magneto-micelles[17,22] were prepared as expected. When DMF/THF (96.8% DMF) was used for the simultaneous self-assembly of nanoparticles and polymers, magneto-core shell assemblies[34−36] were formed due to the poor solvent−PS interaction, which leads to the segregation of nanoparticles from PS and the unique radial arrangement of nanoparticles. The nanoparticle−solvent interaction also affects the hybridization of nanoparticles in polymer assemblies. Due to the poor solvent−nanoparticle interactions, two different sized nanoparticles were segregated into different polymer assemblies when DMF/THF (96.8% DMF) was used as the initial solvent, while in THF, polymer micelles with mixed nanoparticles were formed.

The initial solvent of dioxane/THF (96.8% dioxane) produced magneto-micelles and magneto-polymersomes in varying ratios depending on the polymer length. At low nanoparticle mass percents, vesicle-forming block-copolymers (PAA_{38}-*b*-PS_{154}) produced magneto-micelles instead of magneto-polymersomes because nanoparticles solubilized into the core of polymer assemblies reduce the polymer stretching. At high nanoparticle mass percents, the same polymer produced the mixture of magneto-polymersomes and magneto-micelles due to the nanoparticle-induced change in the relative volume ratio between hydrophobic block and hydrophilic block. The same phenomena occurred for shorter polymers (PAA_{38}-*b*-PS_{73}), which formed micelles without nanoparticles under the same condition. When micelle-forming polymers were self-assembled with nanoparticles, magneto-polymersomes emerged even at very low nanoparticle mass percents (10.0%) along with magneto-micelles. At the nanoparticle mass percent of 35.8%, magneto-polymersomes were the only species. The added hydrophobic nanoparticles effectively increase the volume taken up by the hydrophobic block, making the polymer more symmetric and appropriate for the vesicle formation, which causes the micelle-to-vesicle morphology change.

Importantly, we showed that the self-assembly structure and nanoparticle arrangement significantly affects the spin−spin relaxation rates. The magneto-core shell assemblies showed a significantly higher relaxivity rate than typical magneto-micelles due to the better nanoparticle packing and water accessibility. Magneto-polymersomes showed higher relaxivity rates among all three assemblies because they have a larger number of nanoparticles per assembly and better water accessibility. The magneto-polymersomes formed with PAA_{38}-*b*-PS_{73} at 35.8% nanoparticle mass percent exhibited a higher relaxivity rate than previously reported values[4] for the similar sized nanoparticles.

This study is important for the following reasons. First, we elucidated how nanoparticles affect the self-assembly structure of amphiphilic block-copolymers and nanoparticles. Despite the intense interest in the synthesis of multifunctional nanoparticles through the self-assembly of block-copolymers and nanoparticles, little is known about the impact of nanoparticles on the self-assembly process and resulting structures. The findings in this study will allow one to form hybrid structures with desired morphology and properties. Second, we showed how to control nanoparticle arrangement in the polymer matrix by manipulating the solvent−nanoparticle and polymer−nanoparticle interactions. We also demonstrated for the first time that the arrangement of nanoparticles significantly affects the magnetic relaxivity rates, and we were able to generate self-assembled structures possessing a higher relaxivity rate than previously reported values. Third, it is worth noting that the nanoparticles used in this study are prepared by the common synthetic procedure, and they were self-assembled with polymers without further surface modification. This simplifies the procedure and reduces the change of sample degradation. In addition, typical synthetic methods for many other types of organic phase nanoparticles including the magnetic particles used in this study utilize long chain aliphatic molecules as the stabilizing agent.[54] Thus, the findings in the study should be extended to many different types of commonly synthesized nanoparticles. Finally, the magneto-polymersomes developed in this study possess the highest nanoparticle density reported to date. We believe that they will open up many exciting opportunities in the field of nanomedicine owing to their ability to load both hydrophilic and hydrophobic substances, the controllable nanoparticle density, and the high magnetic relaxivity rate.

ASSOCIATED CONTENT

Supporting Information. Detailed experimental procedures, TEM images of iron oxide nanoparticles, additional EDS and DLS data, a table of physical properties of solvents and polymers used in this study, powder X-ray diffraction patterns, electron diffraction patterns, and zero-field cooling SQUID data of iron oxide nanoparticles and magneto-polymersomes. This material is available free of charge via the Internet at http://pubs.acs.org.

AUTHOR INFORMATION

Corresponding Author
sojungp@sas.upenn.edu

ACKNOWLEDGMENT

S.-J.P. acknowledges support from the MRSEC seed award at Penn (NSF DMR 05-20020), NSF career award (DMR 0847646), and the ARO young investigator award (W911NF-09-1-0146). J.M.K. acknowledges the support from the MRSEC at Penn (NSF DMR 05-20020). The STEM and EDS measurements were carried out using instrumentation at the Penn Regional Nanotechnology Facility. The authors thank Dr. Doug Yates for helpful discussions on the TEM analysis. The authors thank Dr. Adrew Tsourkas and his group for their help with the relaxometer and DLS. The authors thank Dr. David Vann for his help with the ICP. The authors thank Jing Cai for the assistance with magnetic measurements and analysis.

REFERENCES

(1) Arruebo, M.; Fernandez-Pacheco, R.; Ibarra, M. R.; Santamaria, J. *Nano Today* **2007**, *2*, 22–32.
(2) Josephson, L.; Perez, J. M.; Weissleder, R. *Angew. Chem., Int. Ed.* **2001**, *40*, 3204–3206.
(3) Jun, Y. W.; Seo, J. W.; Cheon, A. *Acc. Chem. Res.* **2008**, *41*, 179–189.
(4) Na, H. B.; Song, I. C.; Hyeon, T. *Adv. Mater.* **2009**, *21*, 2133–2148.
(5) Pankhurst, Q. A.; Connolly, J.; Jones, S. K.; Dobson, J. *J. Phys. D: Appl. Phys.* **2003**, *36*, R167–R181.
(6) Perez, J. M.; Josephson, L.; O'Loughlin, T.; Hogemann, D.; Weissleder, R. *Nat. Biotechnol.* **2002**, *20*, 816–820.
(7) Sun, C.; Lee, J. S. H.; Zhang, M. Q. *Adv. Drug Delivery Rev.* **2008**, *60*, 1252–1265.
(8) Sun, S.; Zeng, H. *J. Am. Chem. Soc.* **2002**, *124*, 8204–8205.
(9) Sun, S.; Zeng, H.; Robinson, D. B.; Raoux, S.; Rice, P. M.; Wang, S. X.; Li, G. *J. Am. Chem. Soc.* **2003**, *126*, 273–279.
(10) Park, J.; An, K. J.; Hwang, Y. S.; Park, J. G.; Noh, H. J.; Kim, J. Y.; Park, J. H.; Hwang, N. M.; Hyeon, T. *Nat. Mater.* **2004**, *3*, 891–895.
(11) Kim, J.; Kim, H.; Lee, N.; Kim, T.; Kim, H.; Yu, T.; Song, I.; Moon, W.; Hyeon, T. *Angew. Chem., Int. Ed.* **2008**, *47*, 8438–8441.
(12) Lee, J. E.; Lee, N.; Kim, H.; Kim, J.; Choi, S. H.; Kim, J. H.; Kim, T.; Song, I. C.; Park, S. P.; Moon, W. K.; Hyeon, T. *J. Am. Chem. Soc.* **2010**, *132*, 552–557.
(13) Tan, H.; Xue, J. M.; Shuter, B.; Li, X.; Wang, J. *Adv. Funct. Mater.* **2010**, *20*, 722–731.
(14) Thomas, C. R.; Ferris, D. P.; Lee, J.-H.; Choi, E.; Cho, M. H.; Kim, E. S.; Stoddart, J. F.; Shin, J.-S.; Cheon, J.; Zink, J. I. *J. Am. Chem. Soc.* **2010**, *132*, 10623–10625.
(15) Ai, H.; Flask, C.; Weinberg, B.; Shuai, X.; Pagel, M. D.; Farrell, D.; Duerk, J.; Gao, J. M. *Adv. Mater.* **2005**, *17*, 1949–1952.
(16) Berret, J. F.; Schonbeck, N.; Gazeau, F.; El Kharrat, D.; Sandre, O.; Vacher, A.; Airiau, M. *J. Am. Chem. Soc.* **2006**, *128*, 1755–1761.
(17) Kim, B. S.; Qiu, J. M.; Wang, J. P.; Taton, T. A. *Nano Lett.* **2005**, *5*, 1987–1991.
(18) Kim, B. S.; Taton, T. A. *Langmuir* **2007**, *23*, 2198–2202.
(19) Lecommandoux, S.; Sandre, O.; Chécot, F.; Rodriguez-Hernandez, J.; Perzynski, R. *Adv. Mater.* **2005**, *17*, 712–718.
(20) Lee, J. H.; Huh, Y. M.; Jun, Y.; Seo, J.; Jang, J.; Song, H. T.; Kim, S.; Cho, E. J.; Yoon, H. G.; Suh, J. S.; Cheon, J. *Nat. Med.* **2007**, *13*, 95–99.
(21) Martina, M. S.; Fortin, J. P.; Menager, C.; Clement, O.; Barratt, G.; Grabielle-Madelmont, C.; Gazeau, F.; Cabuil, V.; Lesieur, S. *J. Am. Chem. Soc.* **2005**, *127*, 10676–10685.
(22) Niu, D. C.; Li, Y. S.; Ma, Z.; Diao, H.; Gu, J. L.; Chen, H. R.; Zhao, W. R.; Ruan, M. L.; Zhang, Y. L.; Shi, J. L. *Adv. Funct. Mater.* **2010**, *20*, 773–780.
(23) Tromsdorf, U. I.; Bigall, N. C.; Kaul, M. G.; Bruns, O. T.; Nikolic, M. S.; Mollwitz, B.; Sperling, R. A.; Reimer, R.; Hohenberg, H.; Parak, W. J.; Forster, S.; Beisiegel, U.; Adam, G.; Weller, H. *Nano Lett.* **2007**, *7*, 2422–2427.
(24) Wu, H.; Zhu, H.; Zhuang, J.; Yang, S.; Liu, C.; Cao, Y. *Angew. Chem., Int. Ed.* **2008**, *47*, 3730–3734.
(25) Zhu, J. T.; Hayward, R. C. *J. Am. Chem. Soc.* **2008**, *130*, 7496–7502.
(26) Kim, J.; Piao, Y.; Hyeon, T. *Chem. Soc. Rev.* **2009**, *38*, 372–390.
(27) Cui, H.; Chen, Z.; Zhong, S.; Wooley, K. L.; Pochan, D. J. *Science* **2007**, *317*, 647–650.
(28) Discher, B. M.; Bermudez, H.; Hammer, D. A.; Discher, D. E.; Won, Y.-Y.; Bates, F. S. *J. Phys. Chem. B* **2002**, *106*, 2848–2854.
(29) Discher, B. M.; Won, Y.-Y.; Ege, D. S.; Lee, J. C. M.; Bates, F. S.; Discher, D. E.; Hammer, D. A. *Science* **1999**, *284*, 1143–1146.
(30) Discher, D. E.; Eisenberg, A. *Science* **2002**, *297*, 967–973.
(31) Hayward, R. C.; Pochan, D. J. *Macromolecules* **2010**, *43*, 3577–3584.
(32) Smith, D.; Pentzer, E. B.; Nguyen, S. T. *Polym. Rev.* **2007**, *47*, 419–459.
(33) Gao, X.; Cui, Y.; Levenson, R. M.; Chung, L. W. K.; Nie, S. *Nat. Biotechnol.* **2004**, *22*, 969–976.
(34) Hickey, R. J.; Sanchez-Gaytan, B. L.; Cui, W. H.; Composto, R. J.; Fryd, M.; Wayland, B. B.; Park, S. J. *Small* **2010**, *6*, 48–51.
(35) Kamps, A. C.; Sanchez-Gaytan, B. L.; Hickey, R. J.; Clarke, N.; Fryd, M.; Park, S.-J. *Langmuir* **2010**, *26*, 14345–14350.
(36) Sanchez-Gaytan, B. L.; Cui, W. H.; Kim, Y. J.; Mendez-Polanco, M. A.; Duncan, T. V.; Fryd, M.; Wayland, B. B.; Park, S. J. *Angew. Chem., Int. Ed.* **2007**, *46*, 9235–9238.
(37) Ghoroghchian, P. P.; Frail, P. R.; Susumu, K.; Blessington, D.; Brannan, A. K.; Bates, F. S.; Chance, B.; Hammer, D. A.; Therien, M. J. *Proc. Natl. Acad. Sci. U.S.A.* **2005**, *102*, 2922–2927.
(38) Mabrouk, E.; Cuvelier, D.; Brochard-Wyart, F.; Nassoy, P.; Li, M. H. *Proc. Natl. Acad. Sci. U.S.A.* **2009**, *106*, 7294–7298.
(39) Robbins, G. P.; Jimbo, M.; Swift, J.; Therien, M. J.; Hammer, D. A.; Dmochowski, I. J. *J. Am. Chem. Soc.* **2009**, *131*, 3872–3874.
(40) Mueller, W.; Koynov, K.; Fischer, K.; Hartmann, S.; Pierrat, S.; Basché, T.; Maskos, M. *Macromolecules* **2008**, *42*, 357–361.
(41) Binder, W. H.; Sachsenhofer, R.; Farnik, D.; Blaas, D. *Phys. Chem. Chem. Phys.* **2007**, *9*, 6435–6441.
(42) Krack, M.; Hohenberg, H.; Kornowski, A.; Lindner, P.; Weller, H.; Förster, S. *J. Am. Chem. Soc.* **2008**, *130*, 7315–7320.
(43) Mai, Y.; Eisenberg, A. *J. Am. Chem. Soc.* **2010**, *132*, 10078–10084.
(44) Kang, Y. J.; Taton, T. A. *Angew. Chem., Int. Ed.* **2005**, *44*, 409–412.
(45) Geng, Y.; Discher, D. E. *J. Am. Chem. Soc.* **2005**, *127*, 12780–12781.
(46) Giacomelli, C.; Schmidt, V.; Aissou, K.; Borsali, R. *Langmuir* **2010**, *26*, 15734.
(47) Savic, R.; Luo, L. B.; Eisenberg, A.; Maysinger, D. *Science* **2003**, *300*, 615–618.
(48) Yu, Y.; Zhang, L.; Eisenberg, A. *Macromolecules* **1998**, *31*, 1144–1154.
(49) Zhang, L.; Eisenberg, A. *J. Am. Chem. Soc.* **1996**, *118*, 3168–3181.
(50) Zhang, L. F.; Eisenberg, A. *Polym. Adv. Technol.* **1998**, *9*, 677–699.
(51) Park, M. J.; Park, J.; Hyeon, T.; Char, K. *J. Polym. Sci., Part B: Polym. Phys.* **2006**, *44*, 3571–3579.
(52) Shen, H. W.; Eisenberg, A. *Macromolecules* **2000**, *33*, 2561–2572.
(53) Bockstaller, M. R.; Mickiewicz, R. A.; Thomas, E. L. *Adv. Mater.* **2005**, *17*, 1331–1349.
(54) Peng, Z. A.; Peng, X. *J. Am. Chem. Soc.* **2001**, *123*, 183–184.